Desalination and Water Treatment
www.deswater.com
doi: 10.5004/dwt.2023.30208

316 (2023) 383–394
December

Adsorption properties for ammonia nitrogen by polyacrylic acid/sodium alginate-based titanium dioxide composite hydrogel

Chang-Zi Guo*, Yi Han, Wan-Qin Zhao, Xu-Li Zhang

School of Environmental Science and Engineering, Shaanxi University of Science and Technology, Xi'an 710021, China, Tel.: +8613649201248; emails: guochangzi@sust.edu.cn (C.-Z. Guo), howie778@163.com (Y. Han), zwq602553207@163.com (W.-Q. Zhao), zxl51515@163.com (X.-L. Zhang)

Received 28 September 2023; Accepted 4 December 2023

ABSTRACT

Polyacrylic acid/sodium alginate-based titanium dioxide (PAA/SA@TiO_2) composite hydrogel has the good nitrogen removal properties in the nitrogen-containing wastewaters. Under the optimal adsorption conditions, which include pH 7, temperature 35°C, adsorbent dosage 6 g/L, adsorption equilibrium time 70 min, the adsorption efficiency is 85.56%, 79.46%, and 67.63% when the initial ammonia nitrogen concentrations of 100, 200, and 300 mg/L, respectively, indicating that the hydrogel has good adsorption performance for ammonia nitrogen. The adsorption process conforms to the monolayer adsorption of the Langmuir model, and the adsorption kinetic process belongs to the pseudo-second-order kinetic model of chemical adsorption. The structure of PAA/SA@TiO_2 composite hydrogel is stable. The thermogravimetric analysis revealed that its main chain of the composite hydrogel began to break and degrade only at 446°C with thermally decomposed hydroxyl and carboxyl groups. At 800°C, the thermal loss rate was 48%. After 5 cycles of adsorption regeneration, the adsorption efficiency only drops by about 10%. The research results showed that PAA/SA@TiO_2 composite hydrogel had great application prospects in the field of nitrogen-containing wastewater treatment, which provided the theoretical basis and operating parameters for the hydrogel applying in the nitrogen-containing wastewaters treatment.

Keywords: Composite hydrogel; Ammonia nitrogen; Adsorption mechanism; Performance characterization; Recycling

1. Introduction

In many industrial production processes, nitrogen-containing compounds were commonly used as raw materials, such as leather, chemical, and pharmaceutical industries, which discharge a large amount of high nitrogen-containing wastewaters with serious environmental pollution [1–3]. Nitrogen is an essential nutrient element for agricultural production and the maintenance of ecosystem functions. However, excessive nitrogen in waterbody could lead to the death of aquatic organisms and pose a threat to the environment. In the natural environment, nitrogen pollutants in wastewater mainly existed in the form of ammonia nitrogen [4]. At present, there are approximately 20 million tons of ammonia nitrogen in China's nitrogen-containing wastewaters every year, which was equivalent to 19% of ammonia synthesized through Haber Bosch [5,6]. It was predicted that by 2050, the annual emission of ammonia nitrogen in wastewaters would increase to 35 million tons [7].

At present, the main treatment process for nitrogen-containing wastewater is biological nitrification and denitrification, which means that ammonia nitrogen was firstly biologically oxidized (nitrified) to NO_3^- or NO_2^- under aerobic conditions, and then the oxidized nitrogen was reduced (denitrification) to nitrogen (N_2) under anaerobic conditions [8]. This traditional biological denitrification technology

* Corresponding author.

had mature processes and high nitrogen removal efficiency. However, this process required a large amount of oxygen and carbon sources, resulting in high energy consumption; At the same time, the denitrification process also generated a large amount of CO_2 and NO_x, exacerbating the greenhouse effect. With the implementation of the strategic goal of "carbon peaking and carbon neutrality", the traditional biological denitrification technologies were not compatible with environmental policies in the new environmental protection situation, and the sustainable nitrogen removal processes need to be researched and developed. Among them, ammonia nitrogen recovery was the most desirable method, which could achieve waste resource utilization while wastewater treatment.

Hydrogel was a three-dimensional network structure formed by cross-linking hydrophilic polymers [9]. Because of its large free space between the cross-linking network and the hydrophilic polymer components, the hydrogel had a strong water absorption capacity and could absorb water hundreds to thousands of times higher than its own mass, while the hydrogel itself was insoluble in water [10,11]. In addition, in the process of water absorption, hydrogels could adsorb pollutants (mainly cationic pollutants) through complexation, covalent bonds, electrostatic interactions and even physical adhesion. Therefore, it was easy to regenerate and did not require a large number of chemical regeneration agents [12].

Acrylic was an organic synthetic raw material and synthetic resin monomer composed of vinyl and carboxyl groups. It was the simplest unsaturated carboxylic acid with a very fast polymerization speed, and it was also one of the synthetic hydrogel monomer. For example, Yi et al. [13] polyacrylate hydrogel was prepared by free radical polymerization to remove uranium(VI) from wastewater, with a maximum adsorption capacity of 445.11 mg/g. Sodium alginate (SA) was an anionic natural, biodegradable and renewable biopolymer composed of poly-b-1,4-mannose acid (M unit) and a-1,4-L-glucuronic acid (G unit) in different proportions through 1-4 links. Alginate had been widely used in various commercial and industrial applications, such as cosmetics, food and heavy metal adsorbents [14]. Huang et al. [15] prepared sodium alginate-*g*-sodium acrylate/NaAlg-PNaA/APT composite hydrogel as an adsorbent, adsorbing Cu^{2+} and Zn^{2+} in wastewater solutions, with a maximum adsorption capacity of 343.64 mg/g and 307.46 mg/g, respectively. Sabaa et al. [16] synthesized alginate and poly(2-hydroxyethyl methacrylate) physical hydrogel showed excellent removal ability from alkaline dyes and heavy metal ions. At the same time, SA has the characteristic of easy aggregation, which can easily cause uneven synthesis of materials and lead to synthesis failure during the material synthesis process. FH and SA both have the disadvantage of easy aggregation. Yang et al. [17] found that adding SA to pyrite (FH) can improve the aggregation and non-mobility of FH, thereby enhancing the stability of FH colloidal system. Meanwhile, Liu et al. [18] found that compared with commonly used ferric chloride, the pre-coordinated iron in heme chloride is less prone to aggregation during high-temperature synthesis, which leads to higher dispersion and better uniformity of Fe-SA sites. Overall, it indicates that SA can improve its tendency to agglomerate by adding modifiers.

However, at this stage, the adsorption performance of physical hydrogel and chemical hydrogel was limited. Inorganic nanoparticles had a pore-making effect, which could increase the specific surface area and porosity of the hydrogel and increased the adsorption capacity.

TiO_2 was widely used in organic wastewater treatment because of its strong oxidation ability, low cost, low toxicity, long-term thermodynamic stability and unique semiconductor characteristics [19,20]. TiO_2 nanoparticles were considered to be the most promising materials for widespread use. However, TiO_2 nanoparticles were easy to agglomeration and difficult to recover in water, which greatly limited its practical application [21,22]. Therefore, the fixation of TiO_2 on different carriers, such as carbon, graphene, glass, polymers and carbon nanotubes on activated carriers, had been widely studied and great progress had been made in this field [23–25]. Liu et al. [26] added lignin to pyrite (FH) and induced changes in the Fe(III) bonding environment through the complexation of lignin with Fe(III), which affected the aggregation of nanoparticles.

However, there were still some limitations, such as the poor binding force between TiO_2 and the carrier, low compatibility, lack of flexibility, etc., and the carrier was easily damaged. For this reason, hydrogel, as a carrier of nano-photocatalyst, had begun to receive widespread attention [27–29].

Nanoparticle composite hydrogel was currently mainly used for the adsorption of heavy metal ions. By adjusting operating conditions such as pH, salinity and temperature, the interaction strength between hydrogel and metal ions could be enhanced [30–33]. Thakur [34] acrylic grafted sodium alginate titanium dioxide hydrogel nanocomposites were prepared as methyl purple adsorbents, with an adsorption efficiency of 99.6%. The alginate/polyacrylamide/titanium dioxide composite hydrogel prepared by Wu et al. [35] had a certain adsorption effect on methyl orange and methylene blue. Moon et al. [36] prepared poly(vinyl alcohol)/poly(acrylic)/TiO_2/graphene oxide nanocomposite hydrogel by free radical polymerization and condensation reaction, and the treatment effect of alkaline wastewater was improved by photocatalytic characteristics.

At present, there were few studies on the adsorption of ammonium in wastewater by nano-titanium dioxide composite hydrogel. This study synthesized polyacrylic acid/sodium alginate-based titanium dioxide (PAA/SA@TiO_2) hydrogel with potassium persulfate and titanium dioxide as initiators by grafting sodium alginate by acrylic acid and applying it to the recovery of ammonia nitrogen in nitrogen-containing wastewater. Through the analysis of the structure, functional groups, chemical bonds and other characteristics of PAA/SA@TiO_2 hydrogel, its adsorption performance and adsorption mechanism of ammonia nitrogen were studied. On the basis of exploring ammonia nitrogen recovery and resource utilization, it provided new methods and ideas for the treatment of nitrogen-containing wastewater.

2. Materials and methods

2.1. Materials

Acrylic acid (AA, 99%), N,N′-methylene bisacrylamide (MBA, ≥99%), sodium alginate (SA, ≥ 99%), nano-titanium

dioxide (TiO_2, 20 nm) purchased from Aldrich, potassium persulfate (KPS, GR, ≥99.0%), hydrochloric acid (HCl, AR, 37%), sodium hydroxide (NaOH, AR, particles, ≥98.5%), ammonium chloride (NH_4Cl, AR, ≥99%), sodium chloride (NaCl, AR, ≥99%), all chemicals are analytical pure. It can be used without further purification.

2.2. Preparation method of PAA/SA@TiO_2 hydrogel

2.2.1. PAA/SA@TiO_2 composite hydrogel

The composite hydrogel was prepared by co-polymerization under ultrasonic constant temperature oscillation at 70°C. The specific preparation process was as follows: in the presence of hydroxyl radicals generated by potassium persulfate, acrylic acid was added to form a long chain of acrylic acid, and then N,N′-methylenebisacrylamide was added to dissolve completely before adding TiO_2 dispersion. TiO_2 dispersion was obtained by dispersing TiO_2 powder into a certain amount of distilled water and ultrasonic treatment for 2 h. Heat in a 70°C constant temperature water bath for 4 h to polymerize the mixture to form gel. Soak the obtained hydrogel in 1 M NaOH for 2 h, and then wash the impurities on the surface of gel with distilled water. Finally, dry to a constant weight in a 105°C constant temperature drying oven and store for future use (Fig. 1a). At the same time, acrylic acid/sodium alginate hydrogel PAA/SA (Fig. 1b) was also prepared as a control. As shown in Fig. 1, PAA/SA@TiO_2 the surface of PAA/SA is more porous than that of PAA/SA, because the pore making effect increases the pore size of the hydrogel surface.

2.3. Calculated methods of adsorption capacity and adsorption efficiency

The adsorption performance was reflected by adsorption capacity (q, mg/g) and adsorption efficiency (R, %). Their calculated methods are as follows:

$$q = \frac{\left(C_0 - C_t\right)V}{m} \tag{1}$$

$$R = \frac{C_0 - C_t}{C_0} \times 100\% \tag{2}$$

where C_0 is the concentration of NH_4^+ before adsorption (mg/L); C_t is the concentration of remaining NH_4^+ ions in the solution after adsorption (mg/L); V represents the volume of NH_4^+ ion solution (L) and m is the dry weight of the hydrogel sample (g).

2.4. Experiment methods of ammonia adsorption

Took 100 mL of prepared NH_4^+ solution and adjust pH to the desired value using dilute hydrochloric acid or dilute sodium hydroxide solution. Weighed a amount of the hydrogel sample into the NH_4^+ solution in a 250 mL conical flask. Stirred the mixture at 200 r/min at room temperature for a certain time. the adsorption capacity and adsorption rate were calculated according to the ammonium nitrogen concentration before and after adsorption. Initial ammonium nitrogen concentrations of 100, 200, and 300 mg/L were implemented the adsorption experiments, respectively.

3. Results and discussion

3.1. Mechanism synthesis and analysis

In the long chain of acrylic acid, –OH and –Na groups are active sites. In the initiator KPS solution, $S_2O_8^{2-}$ dissociates in H_2O to produce SO_4^-* and OH* radicals. SA is grafted onto the polyacrylic acid chain under the synergistic action of free radicals and active sites, resulting in a graft copolymer. TiO_2 NPs are added as pore forming agents to PAA/SA polymers, and further form cross-linked networks in the presence of MBA. Forming three-dimensional polymers with larger adsorption capacity and larger pores. NH_4^+ ion in wastewater undergoes electrostatic adsorption with a large number of $–COO^–$ groups in synthetic materials, ultimately forming $–COONH_4^+$ compounds.

3.2. Material characterization

3.2.1. Scanning electron microscopy morphology analysis

From the scanning electron microscopy (SEM) appearance (Fig. 3a and b) of PAA/SA hydrogel before adsorption, it could be seen that the surface of the hydrogel prepared before adsorption contained porous structure and a large number of particles and pores after magnification, which

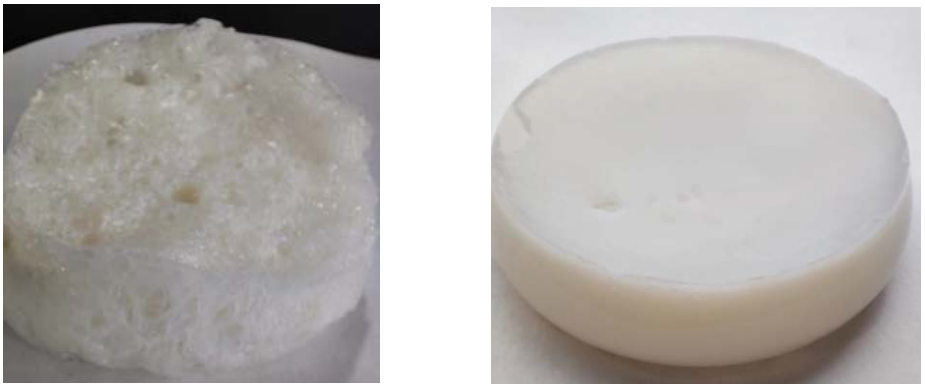

Fig. 1. (a) PAA/SA@TiO_2 and (b) PAA/SA.

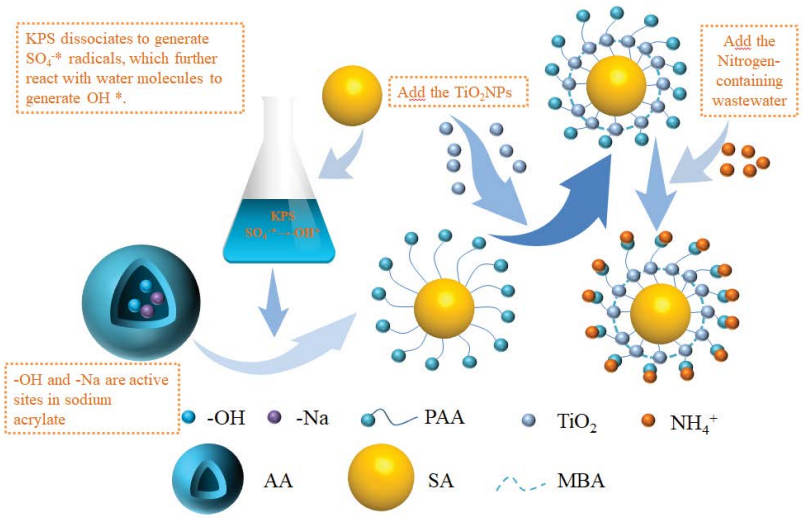

Fig. 2. Mechanism synthesis and analysis.

increased its contact area and had a large number of adsorption points, which could enhance the adsorption of NH_4^+. After the adsorption of ammonia nitrogen, Fig. 3c shows that the surface of PAA/SA hydrogel appeared loose and porous, presumably because the volume of PAA/SA hydrogel increased after water absorption and expansion, while the enlarged Fig. 3d shows that a large number of white particles appeared inside the PAA/SA hydrogel, indicating that ammonia nitrogen was adsorbed into the PAA/SA. Fig. 3e and f show that after adding TiO_2 NPs, a large number of flocs appeared in the hydrogel, and its internal structure was more compact than PAA/SA. However, after the adsorption of ammonia nitrogen, as shown in Fig. 3g and h, the flocs disappear and a large number of white particles are produced, indicating the successful adsorption of ammonia nitrogen.

3.2.2. Fourier-transform infrared spectrogram analysis

PAA/SA and polyacrylic acid (PAA) before and after adsorption/SA@TiO_2 The Fourier-transform infrared spectroscopy characterization analysis results of hydrogel are shown in Fig. 4. The wavelength 3,442 cm^{-1} represents the stretching of –OH group, and the peak at 2,944 cm^{-1} represents the C–H stretching of CH_2 group. 1,561 cm^{-1} belongs to the antisymmetric expansion joint, 1,637 cm^{-1} shows the existence of C=O expansion vibration, and 1,052 cm^{-1} belongs to the C–O expansion joint attributed to the sugar structure of SA. 621 and 1,405 cm^{-1} are characteristic peaks of Ti–O and Ti–O–Ti, respectively. The vibration peak of the adsorbed spectrogram increases at 1,452 cm^{-1}, corresponding to the bending vibration of $–NH_2$, indicating that NH_4^+ has been successfully adsorbed.

3.2.3. Thermogravimetric analysis

The thermogravimetric analysis-derivative thermogravimetry (TG-DTG) curve was used to analyze the thermal stability of PAA. As shown in Fig. 5a, the thermogravimetry of PAA, PAA/SA and PAA/SA@TiO_2 decreased slightly under the condition of normal temperature to 150°C, which was attributed to the fact that the hydrogels of PAA, PAA/SA and PAA/SA@TiO_2 were easy to absorb moisture and the evaporation of residual water molecules in the sample. The heat loss of PAA hydrogel could be divided into three stages. In the first stage, at 150°C–410°C, the heat loss of PAA/SA and PAA/SA@TiO_2 was 6.93%, which could be attributed to the decomposition of N,N′-methylenebisacrylamide in PAA hydrogel and the evaporation of a small amount of potassium persulfate initiator in the hydrogel matrix. The second stage was at 410°C–540°C. In this stage, PAA, PAA/SA and PAA/SA@TiO_2 all decrease rapidly, and the heat loss was 27.09%, 29.42% and 33.42%. The reason was that the main chain of the three hydrogels brought and degraded at this temperature, and the hydroxyl and carboxyl groups were thermally decomposed, while SA and TiO_2 nanoparticles were thermally decomposed, resulting in greater heat loss of the composite PAA/SA@TiO_2. After the third stage of 540°C, the heat loss was still ongoing, and it was speculated that the main reason was the pyrolysis of residual branch chains. Through DTG curve b, it could be found that PAA, PAA/SA, and PAA/SA@TiO_2 undergo the fastest thermal degradation at 440°C–450°C, confirming the conclusion of the second stage mentioned above. Through thermogravimetric analysis, it could be seen that the heat loss of PAA/SA and PAA/SA@TiO_2 hydrogels after composite was increased, but their weight loss rate was still within 50%, which also had good thermal stability.

3.2.4. X-ray photoelectron spectroscopy analysis

The elemental combination state of the composite hydrogel before and after adsorption of NH_4^+ was studied by X-ray photoelectron spectroscopy, and the results are shown in Fig. 6a. PAA/SA and PAA/SA@TiO_2 They all exhibit five binding energy peaks: Cl2p (198.08 eV), C1s (284.36 eV), N1s (399.83 eV), O1s (531.13 eV), and Na1s (1,071.11 eV). PAA/SA@TiO_2 The presence of Ti3s (100.08 eV) and Ti3p (62.08 eV) in the spectrum demonstrates the successful recombination of TiO_2 into PAA/SA@TiO_2 hydrogel. When NH_4^+ ions

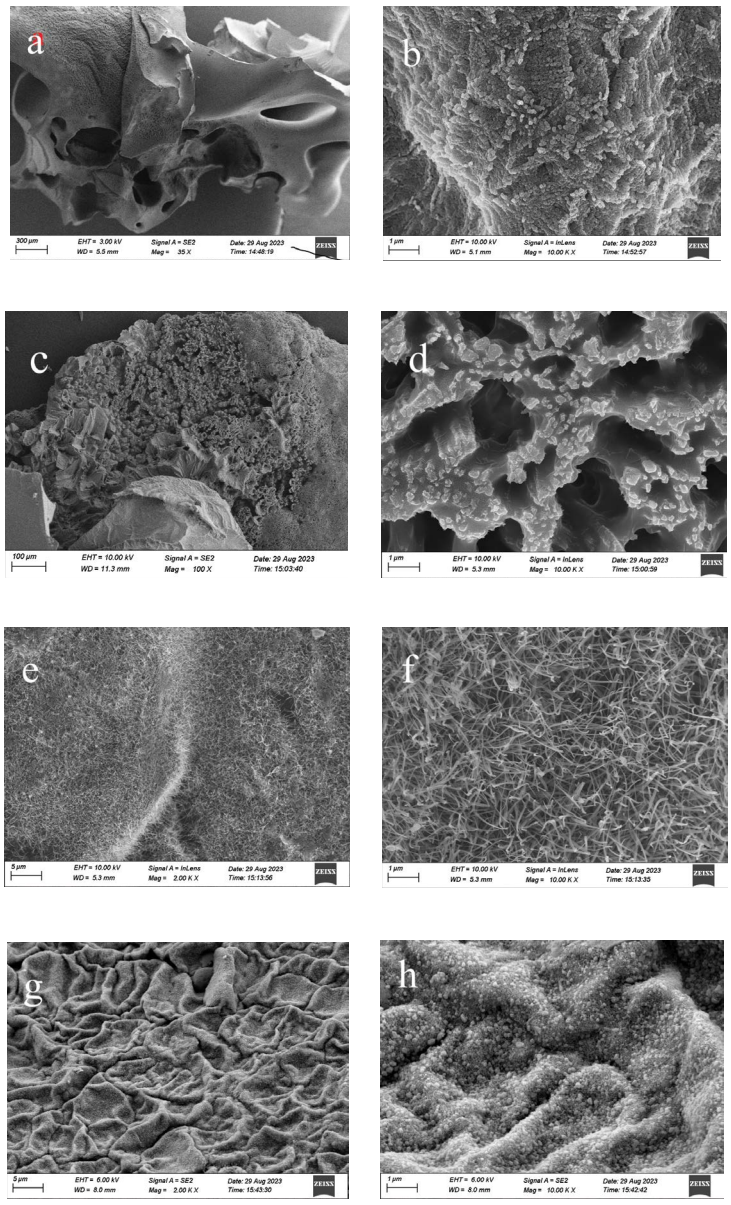

Fig. 3. Scanning electron microscopy morphology of PAA/SA and PAA/SA@TiO_2 hydrogel before and after adsorption: (a,b) before of PAA/SA, (c,d) after of PAA/SA, (e,f) before of PAA/SA@TiO_2, and (g,h) after of PAA/SA@TiO_2.

were adsorbed, the peak at N1s rises and the N content increases, indicating that NH_4^+ was successfully adsorbed into the composite hydrogel. The binding energy information obtained by fitting the peaks of C, N, and O is shown in Fig. 6b and c. In Fig. 6b, a binding energy peak appears at 284.8 eV, attributed to C=C and C–C. The characteristic peak at 286 eV was attributed to C–OH in PAA and SA carboxyl groups, while the binding energy peak at 288.85 eV was attributed to C=O in MBA and O–C=O in PAA carboxyl functional groups. In Fig. 6c, C=O and C–O in the hydrogel appear at 531.5 and 533 eV. The peak plot c of N1s showed $–NH_2^+$, secondary amino (–NH–), and imine (=N–) at 401, 399, and 398 eV, while the binding peak at 397.08 eV was attributed to TiN. After adsorption, $–NH_2^+$ increased, indicating that NH_4^+ was adsorbed onto PAA/SA@TiO_2 medium. The above data indicated that PAA/SA@TiO_2 successfully prepared and had a certain adsorption effect on NH_4^+.

3.3. Influencing factors of ammonia nitrogen adsorption on hydrogel

3.3.1. Adsorption time

To explore the PAA/SA@TiO_2, the best time to adsorb ammonia nitrogen was to simulate the ammonia nitrogen concentration of the influent water as 100, 200, and 300 mg/L, adjusted the pH to 7 with dilute hydrochloric acid and sodium hydroxide, sample and detected the residual ammonia nitrogen concentration at 0, 5, 10, 20, 30, 45, 60, 70, 80, 90 min, and calculated the efficiency of the

hydrogel to adsorb ammonia nitrogen. As shown in Fig. 7, the hydrogel adsorption rate was very fast in the first 30 min, approaching the adsorption peak in 50 min, and reaching the adsorption saturation state after 70 min. The removal rates of ammonia nitrogen solutions with final initial concentrations of 100, 200, and 300 mg/L were stable at 85.56%, 79.46%, and 67.63%, and PAA was determined SA@TiO_2. The best adsorption time of composite hydrogel is 70 min.

3.3.2. pH

Fig. 8 shows the residual ammonia nitrogen concentration after 90 min of adsorption with NH_4^+ concentration of 100 mg/L, adjusted to different pH using sodium hydroxide and hydrochloric acid solutions. The experiment found that when pH = 7, the remaining ammonia nitrogen concentration was the lowest. When pH < 7, there was little change in the remaining ammonia nitrogen concentration. When pH > 7, the concentration of residual ammonia nitrogen increases. It was speculated that the OH* radical produced in alkaline medium reacts with the substrate radical, affecting the chain reaction and destroying the internal structure of the hydrogel. When pH = 11, the remaining ammonia nitrogen concentration only decreases by 40%, and the ammonia nitrogen removal efficiency decreases to the lowest, indicating that PAA/SA@TiO_2. The composite hydrogel was suitable for acid and neutral conditions.

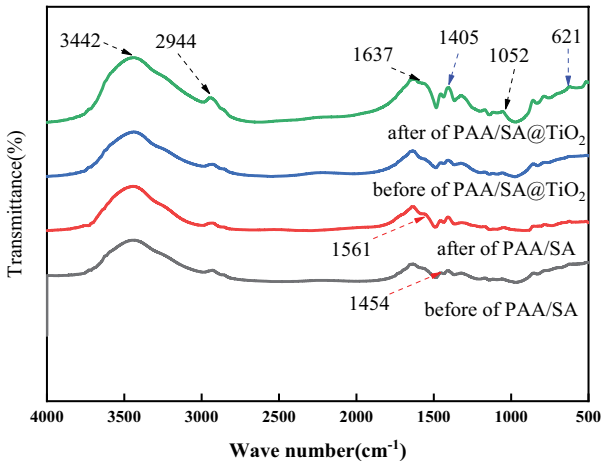

Fig. 4. PAA/SA and PAA/SA@TiO_2 hydrogel Fourier-transform infrared spectrogram of before and after adsorption.

3.3.3. Temperature

Took an appropriate amount of PAA/SA@TiO_2. The composite hydrogel was placed in 50 mL 100 mg/L NH_4^+ solution at 25°C. The adsorption experiments were carried out at 25°C, 30°C, 35°C and 40°C to explore the influence of temperature on the adsorption of NH_4^+ by hydrogels. The results are shown in Fig. 9. From the Fig. 9, it could be seen that the better the adsorption effect is at 35°C, indicating that PAA/SA@TiO_2. The adsorption of composite hydrogel acacia at room temperature was an endothermic process. When the temperature rises to 40°C, PAA/SA@TiO_2. The decrease in adsorption efficiency might be due to the swelling effect of the pore volume inside the adsorbent at high temperatures, which destroyed some hydrogen bonds and leaded to the desorption of some adsorbed NH_4^+ into the solution at high temperatures.

3.3.4. Dosage

As shown in Fig. 10, in 100 mL of NH_4^+ solution, as the adsorbent dosage increased from 1.5 to 10 g/L, the absorption of NH_4^+ increased from 53.5% to 81.8%, followed by no significant change in removal rate. As the dosage increases, the increase in ammonia nitrogen removal rate was due to the increase in adsorption surface area leading to PAA/SA@TiO_2. More available adsorption sites were generated on the hydrogel. There was no significant change in the ammonia nitrogen removal rate when the dosage increased from 6 to 10 g/L. Considering the environmental protection concept of resource conservation, the optimal dosage was determined to be 6 g/L.

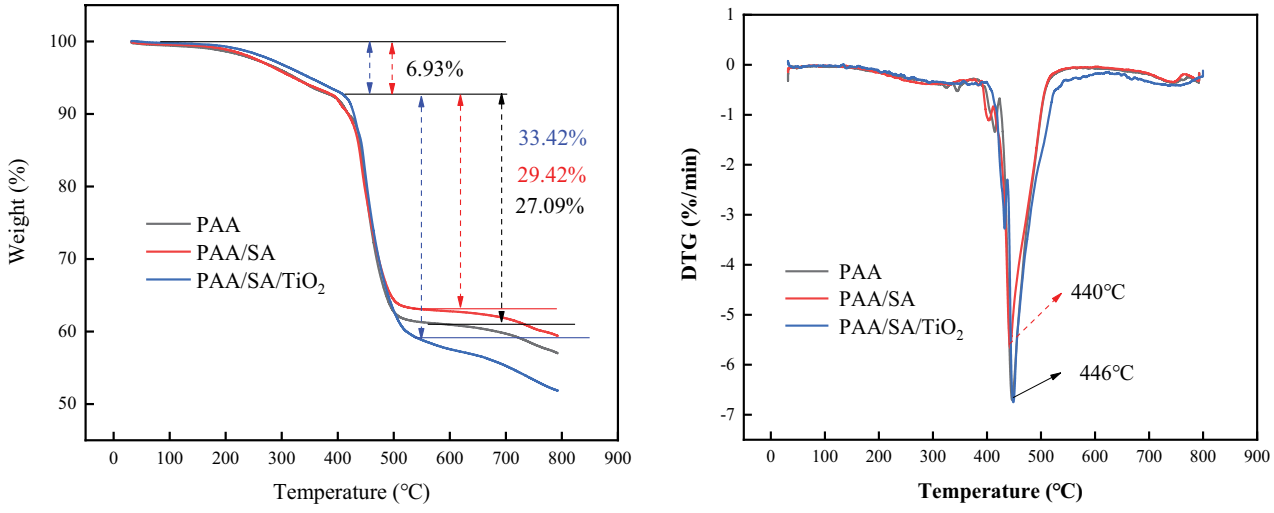

Fig. 5. Thermogravimetric analysis.

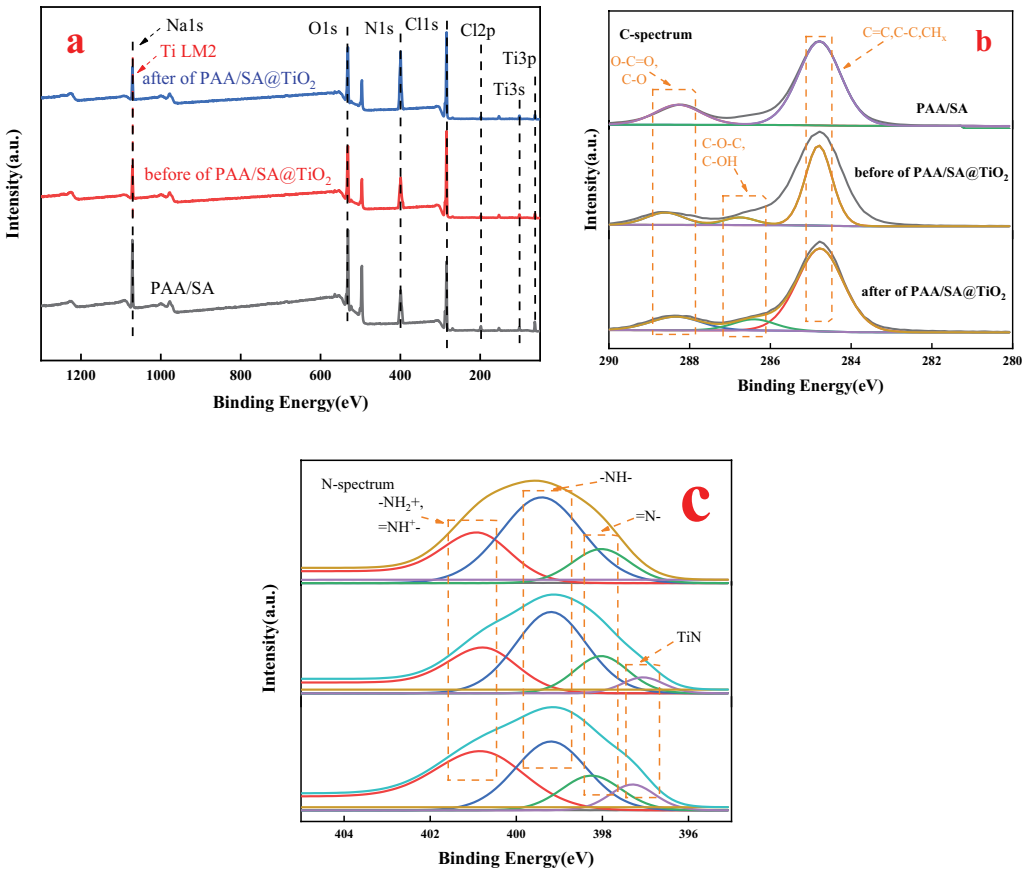

Fig. 6. Hydrogel X-ray photoelectron spectroscopy energy spectrum analysis: (a) X-ray photoelectron spectroscopy total spectrum, (b) C peak fitting, and (c) N peak fitting.

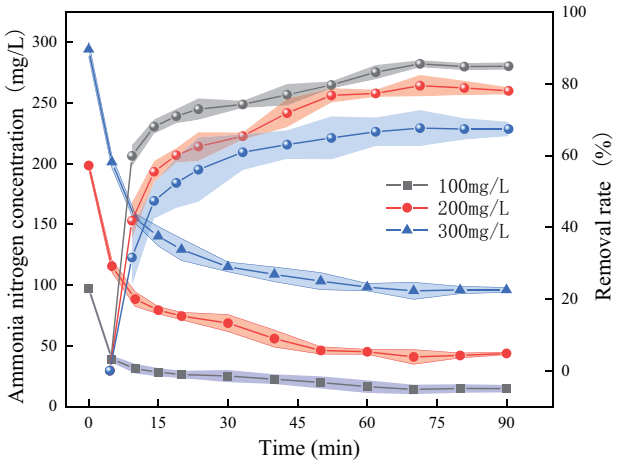

Fig. 7. Effect of adsorption time on the adsorption efficiency of hydrogel.

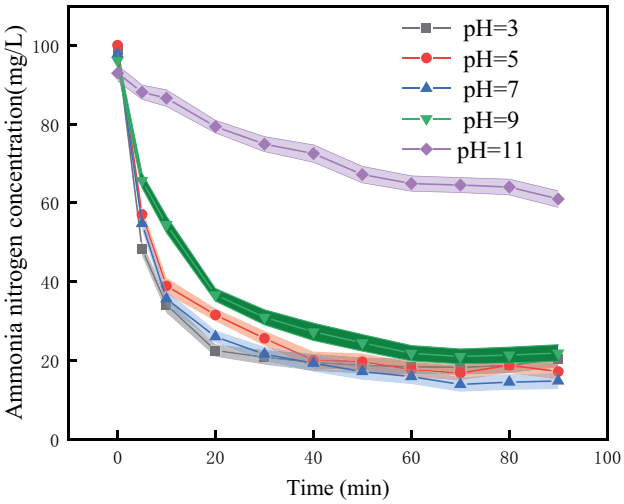

Fig. 8. Effect of pH on the adsorption efficiency of hydrogel.

3.4. Adsorption kinetics and adsorption isotope

3.4.1. Adsorption kinetics

To study the adsorption rate, conducted kinetic studies and reduced experimental errors, determined the initial concentrations of 50, 100, 200, and 300 mg/L, and conducted kinetic experiments at pH = 7 to obtain quasi first and quasi-second-order kinetic model curves and parameters. Fig. 11 shows different initial NH_4^+ concentrations of PAA/SA@TiO_2. The pseudo-first-order kinetic equation and pseudo-second-order kinetic equation of the composite hydrogel adsorption of NH_4^+ are shown in Tables 1 and 2.

From Tables 1, 2, and Fig. 11 it can be seen that the pseudo-first-order and pseudo-second-order kinetic equations fit well with the experimental data of the adsorption curve. In the adsorption test groups with initial NH_4^+ concentrations of 50, 100, 200, and 300 mg/L, the linear correlation coefficient (R^2) of the pseudo-second-order kinetics was greater than that of the pseudo-first-order kinetics equation, and the theoretical equilibrium adsorption amount fitted by

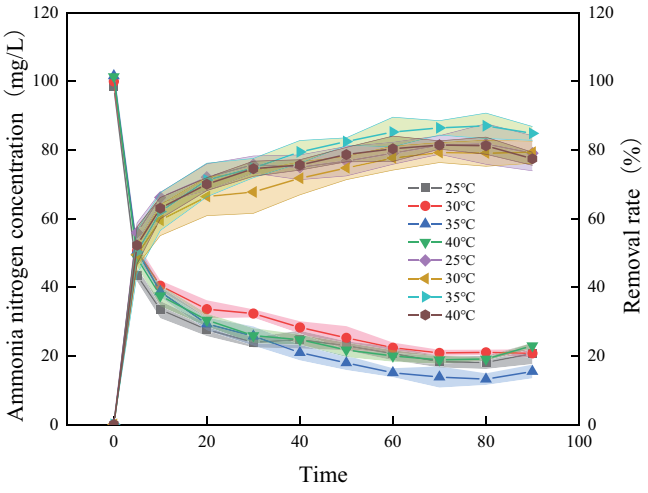

Fig. 9. Effect of temperature on adsorption efficiency of hydrogel.

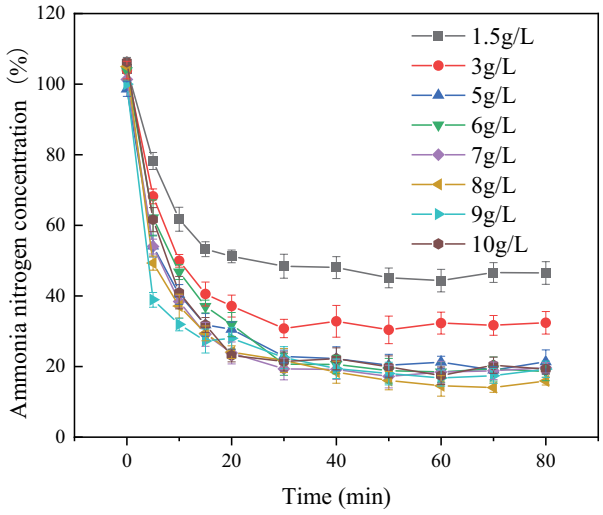

Fig. 10. Effect of dosage on adsorption effect of hydrogel.

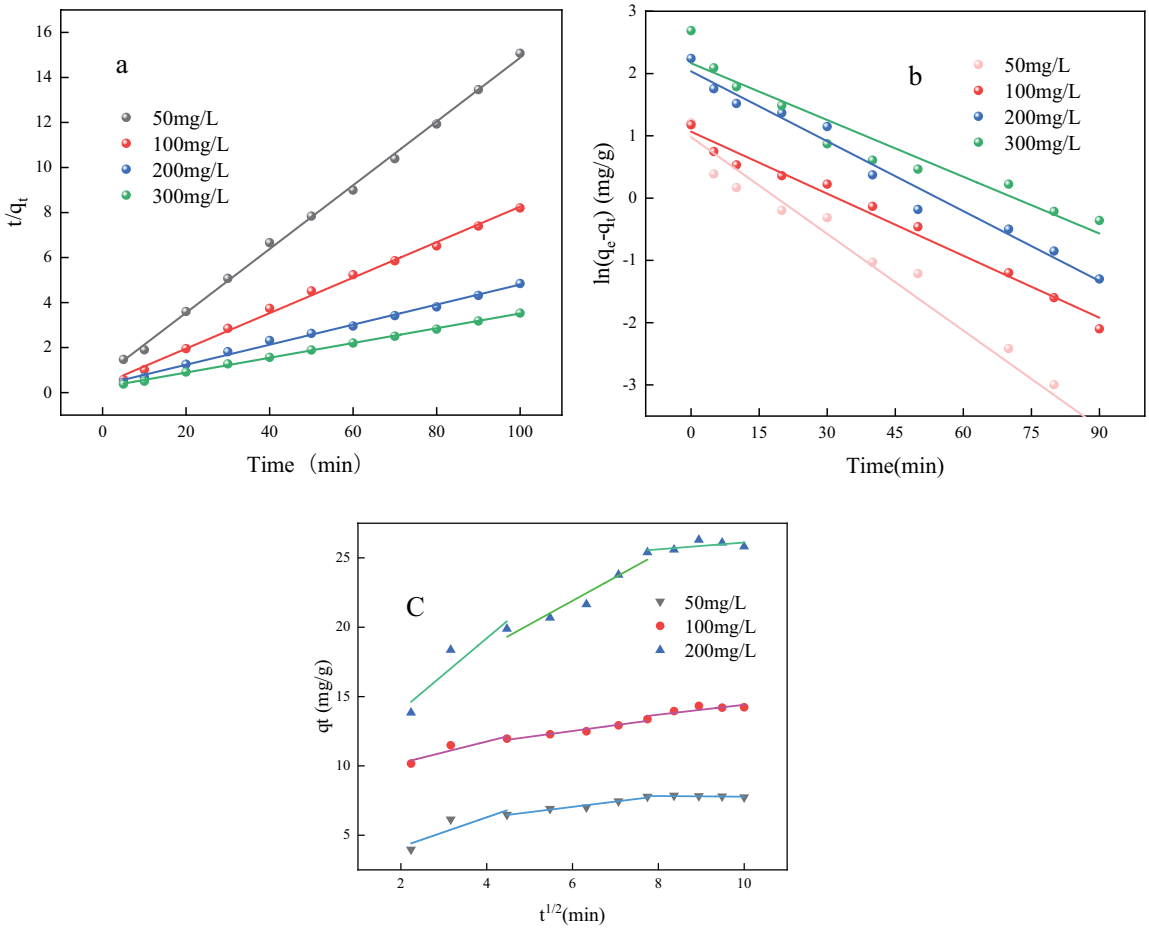

Fig. 11. (a) Quasi-first-order dynamic curve, (b) quasi-second-order dynamic curve, and (c) intraparticle diffusion model.

the pseudo-second-order kinetics equation was closer to PAA/SA@TiO_2. The actual equilibrium adsorption capacity of the composite hydrogel for NH_4^+ indicated that the adsorption process of hydrogel for NH_4^+ was more in line with the pseudo-second-order kinetic model, that was, the adsorption control step was a chemical process.

On the other hand, there was no linear correlation between the adsorption rate constant K of the pseudo kinetic equation and the initial concentration of NH_4^+, indicating that ion exchange and physical adsorption were involved in the adsorption process. The meaning of K value refers to the rate at which the entire adsorption equilibrium reached a special percentage adsorption stage, that was, a larger K value meaned that the adsorption equilibrium could be reached faster. It can be seen from Table 1 that when the initial concentration of NH_4^+ was 50 mg/L, the adsorption rate constant K was the largest, that was, the adsorption energy of hydrogel for NH_4^+ reached the adsorption equilibrium fastest.

In addition, to further clarify PAA/SA@TiO_2, the adsorption mechanism of hydrogel in the process of adsorption of NH_4^+ was simulated by the intraparticle diffusion model of the experimental data. As shown in Fig. 11c, the adsorption reaction rate in the first stage is very fast, mainly under

Table 1
PAA/SA@TiO_2 at different initial concentrations first-order kinetic parameters of hydrogel adsorption

C_0 (mg/L)	$q_{e1,exp}$ (mg/g)	Pseudo-first-order kinetic parameters		
		$q_{e1,cal}$ (mg/g)	K_1 (min^{-1})	R^2
50	7.04	6.66	0.12	0.961
100	13.87	12.90	0.08	0.982
200	26.30	25.65	0.09	0.975
300	33.17	29.72	0.07	0.919

Table 2
PAA/SA@TiO_2 at different initial concentrations second-order kinetic parameters of hydrogel adsorption

C_0 (mg/L)	$q_{e2,cal}$ (mg/g)	K_2 (min^{-1})	R^2
50	7.042	0.028	0.998
100	13.658	0.017	0.996
200	26.222	0.006	0.995
300	33.103	0.005	0.999

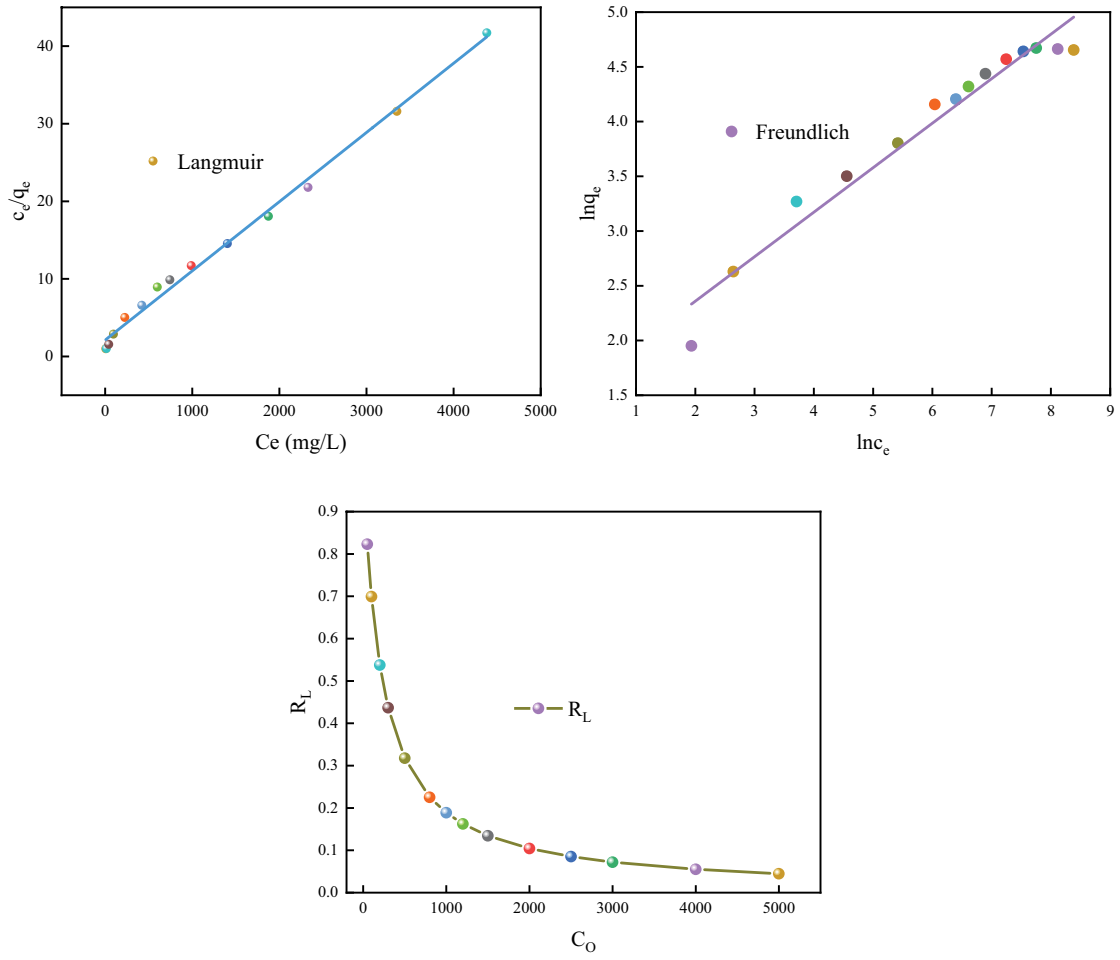

Fig. 12. (a) Langmuir isotherm, (b) Freundlich isotherm, and (c) separation factor (R_L) at different initial concentrations.

Table 3
Intraparticle diffusion models under different initial concentrations

C_0	C_1	K_{id1} (mg/g·min$^{1/2}$)	R_1^2	C_2	K_{id2} (mg/g·min$^{1/2}$)	R_2^2	C_3	K_{id3} (mg/g·min$^{1/2}$)	R_3^2
50	2.016	1.067	0.544	4.741	0.383	0.955	8.011	–0.024	–0.049
100	8.653	0.775	0.746	9.998	0.419	0.946	10.829	0.357	0.569
200	8.792	2.602	0.728	11.689	1.703	0.911	23.639	0.247	0.156

Table 4
Adsorption isotherm model parameters

Experience	q_{exp} (mg/g) = 112.92		
Langmuir	q_m (mg/g)	K_L (L/mg)	R^2
	112.11	0.0043	0.994
Freundlich	n	K_F [(mg/g)(mg/L)$^{-1/n}$]	R^2
	2.463	4.688	0.956

the diffusion effect of the boundary layer, NH_4^+ migrates to PAA through the liquid film SA@TiO_2. The outer surface of the hydrogel is the outer surface adsorption of the adsorbent [37]. The second stage reflects the diffusion of adsorbate into the interior of particles or the inner surface of the adsorbent. The third stage is the adsorption equilibrium stage. As the adsorption time prolongs, the concentration of ammonia nitrogen in the liquid phase decreases, and finally the adsorption reaches equilibrium. The internal diffusion maps under different concentration conditions are composed of multiple straight lines, all of which have not passed through zero points, indicating that membrane diffusion and pore diffusion are jointly involved in the adsorption process.

3.4.2. Adsorption isotherm lines

In order to clearly understand the relationship between adsorption capacity and equilibrium concentration, Langmuir and Freundlich isotherm models were used to fit the experimental data. The adsorption isotherm model and related parameters of hydrogel for NH_4^+ are shown in Fig. 12 and Table 4, respectively. The correlation coefficient of Langmuir model (R^2 = 0.994) was higher than Freundlich's (R^2 = 0.956), and the theoretical maximum adsorption capacity of NH_4^+ fitted by Langmuir model (112.11 mg/g) was close to the experimental maximum adsorption capacity (112.92 mg/g). The results showed that the adsorption process of NH_4^+ by hydrogel was more in line with Langmuir isotherm model, and the adsorption process was in line with monolayer adsorption [38] and the surface-active sites were uniform.

The 1/n values obtained at different concentrations were all less than 1, indicating that the adsorption process of metal ions by adsorbent was good and favorable. How easy it was for the separation factor (R_L) to adsorb NH_4^+. The effect of initial concentration (50–5,000 mg/g) on the separation factor at 25°C was investigated experimentally. From Fig. 12c it can be seen that the range of R_L was from 0.823 to 0.044 ($0 < R_L < 1$), indicating that NH_4^+ had great affinity with PAA/SA@TiO_2 hydrogel.

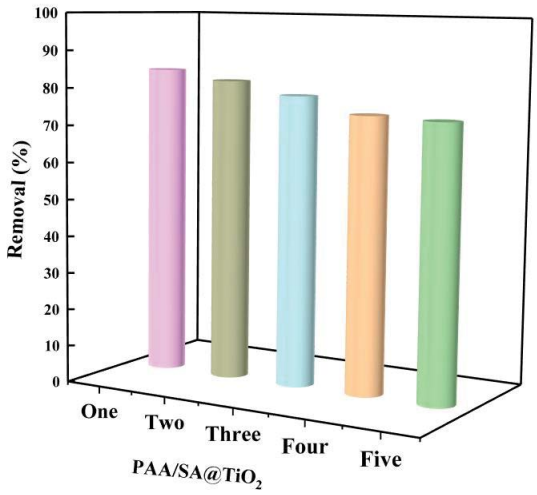

Fig. 13. PAA/SA@TiO_2 hydrogel cycle regeneration adsorption capacity.

3.5. Recycling of adsorbents

From the perspective of economy and resource, the recoverability and reusability of adsorbents were very important. The adsorbed hydrogel was eluted with acid in 0.5 mol/L dilute hydrochloric acid solution for 1 h, then put into 0.5 mol/L sodium hydroxide solution for 2 h for regeneration, and the acid–base solution on the surface was washed with distilled water for many times, and finally put into an oven at 105°C for later use.

The regeneration experiment results are shown in Fig. 13. After five cycles of reuse experiments, the adsorption efficiency of PAA/SA@TiO_2 composite hydrogel decreased from the initial 84.5% to about 74%, which was slightly decreased because NH_4^+ could not be completely desorbed in the desorbing agent, occupying a certain adsorption site. However, the overall downward trend was not significant, indicating that hydrogel had high stability. Adsorbent could be recycled after desorption and drying, so it had potential application prospect in wastewater treatment.

4. Conclusions

(1) PAA/SA@TiO_2 composite hydrogel has the good ammonia nitrogen adsorption properties. The optimal adsorption conditions were pH 7, temperature 35°C, dosage of adsorbent 6 g/L and adsorption equilibrium time

70 min. At the time, the removal efficiencies of ammonia nitrogen were stable at 85.56%, 79.46% and 67.63% for the initial concentration of 100, 200 and 300 mg/L, respectively. The maximum adsorption capacity was 112.92 mg/g.

(2) SEM characterization showed that the surface of PAA/SA@TiO_2 composite hydrogel was uniform and stable, containing porous structure and a large number of particles and pores, which increased its contact area and desorption sites to enhance the adsorption of NH_4^+. After the addition of TiO_2 NPs, a large number of white filaments appeared inside the hydrogel, and its internal structure was more compact than that of PAA/SA. Thermogravimetric analysis showed that the composite hydrogel began pyrolysis only at 446°C, and the heat loss increased at 800°C, but the weight loss rate was still less than 52%, showing good thermal stability of the composite hydrogel.

(3) The ammonia nitrogen adsorption process of PAA/SA@TiO_2 composite hydrogel was monolayer adsorption. The adsorption kinetic process belongs to the pseudo-second-order kinetic model of chemisorption. The intra particle diffusion model indicates that the adsorption is mainly membrane diffusion and pore diffusion. The adsorption efficiency only decreased by about 10% after five cycles of adsorption and regeneration. The composite hydrogel possesses the good adsorption properties and operation stability.

Declaration of interest statement

The authors declare that they have no conflict of interests. We have no financial and personal relationships with other people or organizations with respect to the research, authorship, and publication of this article.

Data availability statement

The dataset generated and analyzed during the current research period can be obtained from the corresponding authors upon reasonable request.

Acknowledgements

This work was financially supported by Natural Science Basic Research Program of Shaanxi Province (Program No. 2023-JC-YB-366), Xi'an Science and Technology Plan Project (Project No. 23GXFW0005), and Shijiazhuang County Special Industry Open Competition Mechanism Science and Technology Project (Project No. 237790722A).

References

[1] J.N. Brown, B.M. Peake, Sources of heavy metals and polycyclic aromatic hydrocarbons in urban stormwater runoff, Sci. Total Environ., 359 (2006) 145–155.
[2] F. Fu, Q. Wang, Removal of heavy metal ions from wastewaters: a review, J. Environ. Manage., 92 (2011) 407–418.
[3] Q. Wang, Z. Yang, Industrial water pollution, water environment treatment, and health risks in China, Environ. Pollut., 218 (2016) 358–365.
[4] M.C.M. Van Loosdrecht, D. Brdjanovic, Anticipating the next century of wastewater treatment, Science, 344 (2014) 1452–1453.
[5] J.W. Erisman, M.A. Sutton, J.N. Galloway, Z. Klimont, W. Winiwarter, How a century of ammonia synthesis changed the world, Nat. Geosci., 1 (2008) 636–639.
[6] J.N. Galloway, E.B. Cowling, Reactive nitrogen and the world: 200 years of change, AMBIO, J. Hum. Environ., 31 (2002) 64–71.
[7] I. Pikaar, S. Matassa, K. Rabaey, B.L. Bodirsky, A. Popp, M. Herrero, W. Verstraete, Microbes and the next nitrogen revolution, Environ. Sci. Technol., 51 (2017) 7297–7303.
[8] R. Brown, C.A. Winkler, The chemical behavior of active nitrogen, Angew. Chem. Int. Ed. in English, 9 (1970) 181–196.
[9] W.Q. Liao, M.H. Zhao, H.W. Rong, P. Jiang, Q. Liao, C.S. Zhang, Y.T. Chen, Photocatalyst immobilized by hydrogel, efficient degradation and self-regeneration: a review, Mater. Sci. Semicond. Process., 150 (2022) 106929, doi: 10.1016/j.mssp.2022.106929.
[10] D. Kanakaraju, F.D. anak Kutiang, Y.C. Lim, P.S. Goh, Recent progress of Ag/TiO_2 photocatalyst for wastewater treatment: doping, co-doping, and green materials functionalization, Appl. Mater. Today, 27 (2022) 101500, doi: 10.1016/j.apmt.2022.101500.
[11] E. Baranowska-Wójcik, D. Szwajgier, P. Oleszczuk, A. Winiarska-Mieczan, Effects of titanium dioxide nanoparticles exposure on human health—a review, Biol. Trace Elem. Res., 193 (2020) 118–129.
[12] N. Kumar, N.S. Chauhan, A. Mittal, S. Sharma, TiO_2 and its composites as promising biomaterials: a review, BioMetals, 31 (2018) 147–159.
[13] X. Yi, Z. Xu, Y. Liu, X. Guo, M. Ou, X. Xu, Highly efficient removal of uranium(VI) from wastewater by polyacrylic acid hydrogels, RSC Adv., 7 (2017) 6278–6287.
[14] C.G. Gomez, M. Rinaudo, M.A. Villar, Oxidation of sodium alginate and characterization of the oxidized derivatives, Carbohydr. Polym., 67 (2007) 296–304.
[15] D. Huang, W. Wang, A. Wang, Removal of Cu^{2+} and Zn^{2+} ions from aqueous solution using sodium alginate and attapulgite composite hydrogels, Adsorpt. Sci. Technol., 31 (2013) 611–623.
[16] M.W. Sabaa, A.M. Ali, S.M.A. Soliman, Physical hydrogel based on alginate and poly(2-hydroxyethyl methacrylate) for water treatment, Desal. Water Treat., 174 (2019) 152–160.
[17] W.H. Yang, Y.J. Zhang, J.H. Zheng, L. Liu, M.Y. Si, Q. Liao, Z.H. Yang, F.P. Zhao, Migration of spent grain-modified colloidal ferrihydrite: Implications for the *in-situ* stabilization of arsenic, lead, and cadmium in co-contaminated soil, Chemosphere, 344 (2023) 140–310.
[18] H. Liu, Y.X. Fu, S.X. Chen, W.C. Zhang, K.S. Xiang, F.H. Shen, R.Y. Xiao, L.Y. Chai, F.P. Zhao, A layered g-C_3N_4 support single-atom Fe-N_4 catalyst derived from hemin to activate PMS for selective degradation of electron-rich compounds via singlet oxygen species, Chem. Eng. J., 474 (2023) 145571, doi: 10.1016/j.cej.2023.145571.
[19] S.M.N. Alam, S. Marzia, M. Atol, I. Sumon, N.R. Fataha, I. Aminul, A.S.M. Sumaia, A review on the development of elemental and co-doped TiO_2 photocatalysts for enhanced dye degradation under UV–vis irradiation, J. Water Process Eng., 47 (2022) 102728, doi: 10.1016/j.jwpe.2022.102728.
[20] Y. Zhao, X.Y. Linghu, Y. Shu, J.W. Zhang, Z. Chen, Y. Wu, D. Shan, B.Q. Wang, Classification and catalytic mechanisms of heterojunction photocatalysts and the application of titanium dioxide (TiO_2)-based heterojunctions in environmental remediation, J. Environ. Chem. Eng., 10 (2022) 108077, doi: 10.1016/j.jece.2022.108077.
[21] A.D. Racovita, Titanium dioxide: structure, impact, and toxicity, Int. J. Environ. Res. Public Health, 19 (2022) 5681, doi: 10.3390/ijerph19095681.
[22] J. Wang, Z. Wang, W. Wang, Synthesis, modification and application of titanium dioxide nanoparticles: a review, Nanoscale, 14 (2022) 6709–6734.
[23] M.H. Alhaji, K. Sanaullah, A. Khan, Recent developments in immobilizing titanium dioxide on supports for degradation of organic pollutants in wastewater-a review, Int. J. Environ. Sci. Technol., 14 (2017) 2039–2052.
[24] A.T. Kuvarega, B.B. Mamba, TiO_2-based photocatalysis: toward visible light-responsive photocatalysts through doping and

fabrication of carbon-based nanocomposites, Crit. Rev. Solid State Mater. Sci., 42 (2017) 295–346.
[25] L.P. Gianluca, B. Awang, K. Duduku, G. Joseph Collin, Preparation of titanium dioxide photocatalyst loaded onto activated carbon support using chemical vapor deposition: a review paper, J. Hazard. Mater., 157 (2008) 209–219.
[26] L. Liu, Z.H. Yang, W.C. Yang, W. Jiang, Q. Liao, M.Y. Si, F.P. Zhao, Ferrihydrite transformation impacted by coprecipitation of lignin: inhibition or facilitation, J. Environ. Sci., 139 (2024) 23–33.
[27] H. Zhu, Z. Li, J. Yang, A novel composite hydrogel for adsorption and photocatalytic degradation of bisphenol A by visible light irradiation, Chem. Eng. J., 334 (2018) 1679–1690.
[28] S. Zhao, C. Hou, L.R. Shao, W.J. An, W.Q. Cui, Adsorption and *in-situ* photocatalytic synergy degradation of 2,4-dichlorophenol by three-dimensional graphene hydrogel modified with highly dispersed TiO_2 nanoparticles, Appl. Surf. Sci., 590 (2022) 153088, doi: 10.1016/j.apsusc.2022.153088.
[29] R. Ratshiedana, A.T. Kuvarega, A.K. Mishra, Titanium dioxide and graphitic carbon nitride–based nanocomposites and nanofibres for the degradation of organic pollutants in water: a review, Environ. Sci. Pollut. Res., 28 (2021) 10357–10374.
[30] E.S. Dragan, Design and applications of interpenetrating polymer network hydrogels: a review, Chem. Eng. J., 243 (2014) 572–590.
[31] J.B. Sytze, W.M.B. Kristel, J.D. Pieter, F.J. Jan, V. Tina, E.H. Wim. Hydrogels in a historical perspective: from simple networks to smart materials, J. Controlled Release, 190 (2014) 254–273.
[32] Y. Zhao, C. Shi, X. Yang, pH- and temperature-sensitive hydrogel nanoparticles with dual photoluminescence for bioprobes, ACS Nano, 10 (2016) 5856–5863.
[33] X.J. Ju, S.B. Zhang, M.Y. Zhou, L.H. Yang, L.Y. Chu, Novel heavy-metal adsorption material: ion-recognition P(NIPAM-*co*-BCAm) hydrogels for removal of lead(II) ions, J. Hazard. Mater., 167 (2009) 114–118.
[34] S. Thakur, O. Synthesis, Characterization and adsorption studies of an acrylic acid-grafted sodium alginate-based TiO_2 hydrogel nanocomposite, Adsorpt. Sci. Technol., 36 (2017) 458–477.
[35] T.M. Wu, A. Sawut, R. Simayi, X.K. Gong, X.H. Zhang, M.H. Jiang, Z.W. Zhu, Green synthesis and environmental applications of alginate/polyacrylamide/titanium dioxide composite hydrogel, J. Appl. Polym. Sci.,140 (2023) e54394, doi: 10.1002/app.54394.
[36] Y.E. Moon, G. Jung, J. Yun, H.I. Kim, Poly(vinyl alcohol)/poly(acrylic acid)/TiO_2/graphene oxide nanocomposite hydrogels for pH-sensitive photocatalytic degradation of organic pollutants, Mater. Sci. Eng., 178 (2013) 1097–1103.
[37] H. Xiang, Z. Yang, S. Liu, Natural pyrite-assisted mechanochemical recovery of insoluble manganese from electrolytic manganese residue: kinetics and mechanisms, ACS ES&T Eng., 10 (2023) 1661–1673.
[38] L Liu, Z.H. Yang, F.P. Zhao, Z.T. Chai, W.C. Yang, H.R. Xiang, Q. Liao, M.Y. Si, Z. Lin, Manganese doping of hematite enhancing oxidation and bidentate-binuclear complexation during As(III) remediation: experiments and DFT calculation, Chem. Eng. J., 471 (2023) 144–758.